HHS Public Access

Author manuscript

Methods Mol Biol. Author manuscript; available in PMC 2020 January 01.

Published in final edited form as:

Methods Mol Biol. 2019 ; 1929: 111–125. doi:10.1007/978-1-4939-9030-6_8.

Designing Calcium-Binding Proteins for Molecular MR Imaging

Mani Salarian[1], **Shenghui Xue**[1,2], **Oluwatosin Y. Ibhagui**[1], and **Jenny J. Yang**[3]

[1]Department of Chemistry, Center for Diagnostics and Therapeutics, Georgia State University, Atlanta, GA, USA.

[2]Inlighta Biosciences, Atlanta, GA, USA.

[3]Department of Chemistry, Center for Diagnostics and Therapeutics, Georgia State University, Atlanta, GA, USA.

Abstract

Early diagnosis, noninvasive detection, and staging of various diseases, remain one of the major clinical barriers to effective medical treatment and prevention of disease progression toward major clinical consequences. Molecular imaging technologies play an indispensable role in the clinical field in overcoming these major barriers. The increasing application of imaging techniques and agents in early detection of different diseases such as cancer has resulted in improved treatment response and clinical patient management. In this chapter we will first introduce criteria for the design and engineering of calcium-binding protein (CaBP) parvalbumin as a *pro*tein Gd-MRI contrast *a*gent (ProCA) with unprecedented metal selectivity for Gd^{3+} over physiological metal ions. We will then discuss the further development of targeted MRI contrast agent for molecular imaging of PSMA biomarker for early detection of prostate cancer.

Keywords

CaBP; Parvalbumin; Molecular imaging; MRI; ProCA; Contrast agent; PSMA

1 Introduction

Magnetic resonance imaging (MRI) is a noninvasive imaging modality providing high-resolution, 3D images of anatomic structures, as well as functional and physiological information about tissues in vivo. MRI has the capacity to detect abnormalities in deep tissues and provide whole-body imaging and, therefore, has been recognized as one of the primary diagnostic imaging techniques [1, 2]. Exogenous MRI contrast agents are usually applied to enhance the contrast between pathological and normal tissues by changing the longitudinal and transverse (i.e., T1 and T2) relaxation times of water protons.

Gd^{3+} chelators have high magnetic moments, asymmetric electronic ground states, and potential for increased MRI contrast; therefore, they are among the most frequently used MRI contrast agents [3, 4]. Relaxivity, defined as the capability of the agent to change the

jenny@gsu.edu.

relaxation time of water, is dependent on several factors such as the number of water molecules in the coordination shell, the exchange rate of the coordinated water with the bulk water, and the rotational correlation time τ_R of the molecule [5, 6].

There are several important criteria for an MRI contrast agent to have: first, they should have high relaxivity for high contrast-to-noise ratio (CNR) and dose efficiency; second, good thermodynamic and chemical stability and especially good metal selectivity for the Gd^{3+} over other physiological metal ions, to avoid the release of toxic Gd^{3+}; third, adequate vascular tissue retention time for optimized imaging time; and fourth, timely excretion from the body.

To date, the most widely used MRI contrast agent in diagnostic imaging is Gd-DTPA (diethylene triamine pentaacetic acid) or related derivatives such as Gd-DTPA-BMA (bismethylamide), which are based on small-molecule Gd^{3+} chelators. These small molecular Gd^{3+} chelators have longitudinal and transverse proton relaxivities, r_1 and r_2, less than 5 mM^{-1} s^{-1} at clinical and high field strength, which are much lower than the theoretically maximal value (>100 mM^{-1} s^{-1}), so they therefore lack sufficient sensitivity [7]. Moreover, these small-molecule contrast agents demonstrate very short blood circulation (less than 30 min) and tissue retention time, limiting their MRI applications [8]. To increase correlation time, τ_R, and therefore their sensitivity, small chelators have been covalently or non-covalently linked to macromolecules such as linear polymers [9], dendrimers [10, 11], carbohydrates [12], proteins [13, 14], viral capsids [15], and liposomes [16]. However, conjugation yields limited improvement due to challenges associated with internal mobility, restricted water-exchange rates, limited applications to imaging biomarkers on the blood vessel because of large size and low tissue penetration, and incomplete elimination from the body resulting in Gd^{3+} toxicity.

Calcium-binding proteins (CaBPs) have been an attractive target in molecular imaging studies since they represent the important role of calcium as a second messenger in different cellular signaling pathways. For instance, fluorescent calcium sensors are widely applied in optical imaging at cellular and cell population levels. Calcium-sensitive dyes combined with laser scanning microscopy have been recently used to monitor neural network activities in small brain areas [17], as well as characterizing patterns of interaction between cells in vertebrate embryos [18]. Until now, however, only very limited cases have reported the application of engineered CaBPs as molecular magnetic resonance imaging (MRI) Gd^{3+} contrast agents, possibly due to challenges associated with the engineering and development of protein-based MRI contrast agents and designing suitable Gd^{3+}-binding sites in these proteins.

We have pioneered the development of a novel class of MRI contrast agents using protein design and engineering. Proteins were investigated as a suitable biomolecule for contrast agent development based on the fact that approximately 1/3 of all proteins are metalloproteins with diversified metal selectivity and biodistribution, and they are biocompatible. Previous studies have also applied shorter peptides, and increases in relaxivity were observed when Gd^{3+} binds to calcium-binding peptides [19] or proteins such as concanavalin A and bovine serum albumin (BSA). However, application of these short

EF-hand peptides or proteins as MRI contrast agents has been limited due to their weak metal-binding affinity for Gd^{3+} (K_d ~100 μM for Eu^{3+}) and lack of dynamic flexibility [19, 20]. Jasanoff and coworkers previously reported calmodulin (CaM) modified superparamagnetic iron oxide (SPIO) nanoparticles as Ca^{2+}-responsive MRI T2 agents, but these constructs lacked the ability to penetrate cell membranes, and effective imaging was limited by the dark contrast associated with the iron oxide nanoparticles [21].

Taking a different approach, work in our laboratory has focused on engineering Gd^{3+}-binding sites in CaBPs to develop Gd^{3+} MRI contrast agents [22–28]. In this chapter, we first report our detailed analysis of metal-binding sites in various natural CaBPs to gain insight into coordination chemistry and metal selectivity. Then, we describe our approach to designing and engineering protein-based contrast agents by creating high coordination Gd^{3+}-binding sites in a stable Ca^{2+}-binding protein using amino acid residues and water molecules as metal coordinating ligands and thereby transforming EF-hand motifs into Gd^{3+}-binding motifs, resulting in MRI contrast agents for molecular imaging of cancer and their biomarkers. The design of Gd^{3+}-binding proteins based on CaBPs for molecular imaging described in this chapter largely relies on the concept of the EF-hand calcium-binding protein (α-parvalbumin), and that will be the focus of the chapter. The protocol will further summarize our methods for biophysical characterization of the engineered protein and development of different metal-binding assays. The designed protein demonstrates a high selectivity for Gd^{3+} over physiological metal ions such as Ca^{2+}, Zn^{2+}, and Mg^{2+}. Moreover, it shows a 20-fold increase in longitudinal and transverse relaxation rate values over clinical small-molecule contrast agents, such as Gd-DTPA. In addition, these contrast agents, designed from CaBPs, have stronger contrast enhancement and much longer blood retention time than Gd-DTPA in mice. With superior in vivo properties, the protein contrast agent ProCA has shown great promise as a molecular imaging probe to target disease biomarkers and extending applications of magnetic resonance imaging (MRI) (Fig. 1).

2 Materials

2.1 Bioinformatic Analysis of Calcium-Binding Sites Based on MUG Algorithm

1. Protein sequence search from NCBI: http://www.ncbi.nlm.nih.gov/protein/.
2. MUltiple Geometries (MUG) algorithm to accurately predict CaBPs with multiple-binding sites that undergo local conformational change or side-chain rotations upon Ca^{2+}-binding: http://chemistry.gsu.edu/faculty/Yang/Calciomics.htm [29].
3. Java program for MUG implementation: http://java.sun.com/.
4. PyMOL, used for molecular visualization: http://pymol.sourceforge.net/.

2.2 Molecular Cloning Reagents

1. Primer phosphorylation: T4 Polynucleotide Kinase (PNK) and PNK buffer (New England Biolabs). ATP (Sigma).

2. PCR: KOD hot start DNA polymerase and buffer (Novagen). dNTP (Novagen). $MgSO_4$ (Novagen).
3. Ligation: T4 DNA ligase and ligation buffer (New England Biolabs). ATP (Sigma).
4. Transformation: Competent cells: DH5α and BL21(DE3) pLysS (Invitrogen). LB broth media and LB agar (EMD Chemicals). Ampicillin (Inalco S.p.A, Milano, Italy).
5. Molecular cloning kits: QIAprep Spin Miniprep Kit and QIA-quick Gel Extraction Kit (Qiagen).

2.3 Protein Expression and Purification

1. Protein expression for α-parvalbumin (ProCA32):$6#Escherichia coli BL21(DE3)pLysS cell strain. Isopropyl β-D-1-thiogalactopyranoside (IPTG) stock solution: 1 M IPTG in ddH_2O, sterilized by injection through a 0.2 μm syringe filter. UV-VIS spectrophotometer (Shimadzu).
2. Protein purification and preparation of α-parvalbumin (ProCA32):

   Sonication and French press. Lysis buffer: 10 mM HEPES, pH 7.2, with 100 μM PMSF and 1 μL of benzonuclease (Novagen). DNA precipitation with 3% (wt/vol) streptomycin sulfate. HiTrap Q column (GE Healthcare). Chelex-100 for metal removal. FPLC (GE Healthcare). ICP-OES (Agilent Technologies). PEGylation buffer: 10 mM HEPES at pH 7.2. PEGylation reagents: trimethyl-PEG-NHS Ester reagent, TMS (PEG) 12 (Thermo Scientific). PEGylation quench buffer: 100 mM Tris–HCl, pH = 8.0.

2.4 Instruments for Biophysical Characterization of Engineered Proteins

QuantaMaster™40 fluorometer (PTI, Birmingham, NJ). Jasco-810 circular dichroism spectropolarimeter (JASCO, Easton, MD). Relaxometer at 1.47 T (Bruker). Stelar Spinmaster Fast Field Cycling NMR spectrometer FFC-2000 (Bruker). ICP-OES (Agilent Technologies).

2.5 Fluorescent-Based Metal-Binding Assays

Metal-binding affinity assays: 10 μM ProCA32, 5 mM EGTA or 5 mM DTPA, 100 mM KCl, 50 mM HEPES at pH 7.2., 10 mM or 20 μM stock solution of $CaCl_2$ or $TbCl_3$.

2.6 Water Coordination Number by Terbium Lifetime Luminescence

10 μM of Tb^{3+}-DTPA, Tb^{3+}-EDTA, Tb^{3+}-NTA, and Tb^{3+}-H_2O, and 10 μM of Tb^{3+}-ProCA in H_2O and D_2O.

2.7 Transmetallation Studies of ProCA32

50 or 100 μM ProCA, 100 μM $GdCl_3$, 100 μM $ZnCl_2$, and 1.2 mM PO_4^{3-} buffer.

3 Methods

3.1 Design of Gd^{3+}-Binding Sitesin α-Parvalbumin

Run MUG algorithm with three major steps:

1. In **step 1**, for any protein with determined holo (bound) structure, locate clusters of oxygen atoms in close proximity to each other in the three-dimensional structure, and treat each cluster as a potential ligand group.
2. In **step 2**, recognize a point CC (calcium center) for the insertion of a calcium ion using a grid algorithm for each oxygen cluster.
3. In the final step, sequentially filter and apply various restrictions to the structure of the (cluster, CC) pair. After passing all filters, the cluster can be a predicted ligand group, and CC is the predicted calcium position [29–32]. This process is summarized in Fig. 2.
4. Develop the protein-based MRI contrast agent (ProCA32) based on rat α-parvalbumin. Parvalbumin has two functional Ca^{2+}-binding sites (CD and EF sites).
5. Achieve the mutations of S56D and F103 W in α-parvalbumin by site-directed mutagenesis.
6. Generate the S56D mutation in the CD site of the protein, and on the amino acid serine, which directly coordinates Ca^{2+} via its main chain oxygen. The replacement of aspartic acid introduces more negative charge in the coordination sphere, increasing the selectivity of Gd^{3+} over Ca^{2+}. In this contrast agent, the affinity of Gd^{3+} was significantly increased. Introduce the F103 W mutation in the EF site for ease of determination of metal-binding affinities by Luminescence Resonance Energy Transfer (LRET).

3.2 ProCA32 Expression and Purification

1. Transform the correct plasmid encoding the engineered protein into BL21(DE3)pLysS competent cells for protein expression. Positive colonies were selected on ampicillin-resistant LB agar plates.
2. Inoculate a single colony into 10 mL LB-amp medium, and shake the culture overnight at 200–250 rpm at 37 °C.
3. Transfer the overnight culture to 1 L fresh LB-amp medium, and allow the culture to grow until the OD_{600} reaches 0.6–0.8.
4. Induce protein expression with 0.3 mM IPTG, and allow the bacteria to grow for another 3–4 h at 200 rpm, 37 °C.
5. Harvest cells by centrifugation at 5000 × *g* for 20 min, and collect the cell pellets in a 50 mL centrifuge tube.
6. Store the cell pellets at −80 °C for future use.

7. Sonicate the cell pellet in 10 mM HEPES buffer, pH 7.2, 100 μM PMSF, and 1 μL of benzonuclease, and then pass it through a French pressure cell.
8. Incubate the supernatant of the cell lysate at 85 °C for 10 min, cool to 4 °C in an ice-water bath, and centrifuge (41,100 × *g*, 20 min, 4 °C).
9. Then precipitate the unwanted components, such as DNA, by addition of 3% (wt/vol) streptomycin sulfate.
10. After dialysis at 4 °C for 24 h against 10 mM HEPES at pH 8.0, purify the protein mixture using a HiTrap Q column.
11. After removing unbound proteins with three column volumes of HEPES at pH 8.0, elute the column with a 0–1 M NaCl gradient in 10 mM HEPES at pH 8.0. Remove metals in ProCA32 by Chelex-100, and analyze metal content in ProCA32 by ICP-OES.

3.3 Structural Analysis of ProCA32

1. Secondary structure analysis by circular dichroism spectroscopy:
2. Acquire the circular dichroism spectrum of the engineered protein with a Jasco-810 spectropolarimeter at ambient temperature using a quartz cell of 1-mm path length. Obtain all spectra as the average of at least 8 scans with a scan rate of 50 nm/min.
    a. Prepare 300 mL of the engineered protein sample with a final concentration of 10–20 mM in 10 mM Tris–HCl at pH 7.4. Transfer ~250 mL to a 1-mm-path-length quartz cuvette.
    b. Record CD spectrum in the far-UV (190–260 nm) range. Adjust the protein concentration until the CD signals are between −10 and −20 mdeg.
    c. Record and use the CD signals from the buffer for back-ground subtraction.
3. 2. NMRD studies of ProCA32:
    a. Conduct magnetic relaxation dispersion experiments over the magnetic field range corresponding to proton Larmor frequencies from 0.01 to 40 MHz at 25 °C.
    b. Regulate the temperature using the Stelar temperature controller to set airflow temperature over the sample.
    c. Measure relaxation rate constants with an automated profile-acquisition procedure using a 20-MHz polarization field and 16 different relaxation delays at each relaxation field, and detect the free induction decay at15.8 MHz following each field cycle.

3.4 ^{17}O NMR Study of ProCA32

Measure the water-exchange rates of ProCA using variable temperature ^{17}O NMR.

a. Prepare 10 μM ProCA containing 20 mM Gd^{3+} in 2% (vol/vol) ^{17}O water with 10 mM HEPES buffer at pH 7.0.

b. Load this solution, or 2% (vol/vol) ^{17}O water without protein, in a spherical NMR bulb, and then insert it into a 5-mm NMR sample tube filled with 400 μL of ddH_2O containing 3% (vol/vol) D_2O.

c. Collect the variable temperature Fourier transform ^{17}O NMR at 54.24 MHz using Bruker 400-MHz NMR spectrometer equipped with broadband probe. Measure the line widths of ^{17}O at different temperatures ranging from 25 to 50 °C.

d. Calculate the reduced transverse relaxation rate ($1/T_{2r}$) by Eqs. (1) and (2):

$$\frac{1}{T_{2r}} = \frac{\pi}{P_m} \times \left(\Delta_{\text{ProCA}} - \Delta_{\text{solvent}}\right) \quad (1)$$

$$P_m = \frac{q \times \left[\text{Gd}^{3+}\right]}{\left[\text{H}_2\text{O}\right]} \quad (2)$$

where P_m is the molar fraction of solvent in the exchanging site compared with bulk water, which you can determine by Eq. (2).

Δ_{ProCA} is the half-width of the ^{17}O NMR signal of solvent in the presence of 10 mM ProCA. Δ_{solvent} denotes the half-width of the ^{17}O NMR signal of solvent without contrast agent, while q is the water coordination number of ProCA32-P40, $[Gd^{3+}]$ is the concentration of Gd^{3+}, and $[H_2O]$ is the water concentration.

e. Fit the water-exchange rate by Eqs. (3)–(5):

$$\frac{1}{T_{2r}} = \frac{1}{\tau_m}\left(\frac{\Delta\omega_m^2}{\tau_m^{-2} + \Delta\omega_m^2}\right) \quad (3)$$

$$\frac{1}{\tau_m} = k_{\text{ex}} = \frac{k_{\text{ex}}^{298} T}{298.15} \exp\left[\frac{\Delta H^{\ddagger}}{R}\left(\frac{1}{298.15} - \frac{1}{T}\right)\right] \quad (4)$$

$$\Delta\omega_m = \frac{A}{T} \quad (5)$$

where k_{ex}^{298} is the water molecule exchange rate at 298.15 K, T is the temperature in Kelvin, $\Delta H^{\ddagger}$ is the enthalpy of activation, R is the universal gas constant, and $\Delta\omega_m$ is the difference between the resonance frequency of ^{17}O nuclei of inner-sphere water and bulk water. Assume that temperature dependence of $\Delta\omega_m$ is the simple reciprocal function of A/T (Eq. 5) [33], where you can determine A as a parameter in the treatment of the line broadening data.

3.5 Metal-Binding Affinity Assays

1. Excitation and emission wavelength setup for metal-binding experiments: \$6#Monitor tryptophan (Trp) fluorescence using excitation at 280 nm and emission between 290 and 370 nm with 2–4 nm bandpasses. Acquire Tb^{3+} LRET data by excitation of tryptophan at 280 nm and emission from 500 to 650 nm.

2. Ca^{2+}-binding affinity determination:

   To calculate Ca^{2+}-binding affinity to ProCA, use a calcium-EGTA buffer system, which contains 50 mM HEPES, 100 mM NaCl, and 5 mM EGTA at pH 7.2. Then, titrate calcium chloride at different concentrations into the buffer system, and calculate the free calcium concentration according to Tsein's method [34] (K_d of EGTA is 1.51×10^{-7} M) using Eq. (6). Calculate the Ca^{2+}-binding affinity for ProCA ($K_{d_{\text{Ca, ProCA}}}$) by fitting Trp fluorescence change over various concentrations of free Ca^{2+} using Eq. (7):

$$\left[Ca^{2+}\right]_{\text{free}} = K_{d_{\text{Ca, EGTA}}} \times \frac{[\text{Ca} - \text{EGTA}]}{[\text{EGTA}]_{\text{free}}} \quad (6)$$

$$f = \frac{\left[Ca^{2+}\right]^n_{\text{free}}}{K_{d^n_{\text{Ca, ProCA}}} + \left[Ca^{2+}\right]^n_{\text{free}}} \quad (7)$$

   where $[Ca^{2+}]_{\text{free}}$ is the free Ca^{2+} concentration at each titration point, $K_{d_{\text{Ca, EGTA}}}$ is the dissociation constant of EGTA for Ca^{2+}, [Ca-EGTA] denotes the concentration of total Ca-EGTA complex at each titration point, f represents fractional change of fluorescent signal, and $[EGTA]_{\text{free}}$ is the concentration of EGTA at each titration point.

3. Tb^{3+}-binding affinity determination:

   Obtain Tb^{3+}-binding affinity for ProCA using a Tb^{3+}-DTPA buffer system. Add 30 μM ProCA into the Tb^{3+}-DTPA buffer system, which contains 5 mM DTPA, 50 mM HEPES, and 100 mM NaCl at pH 7.2. Then, titrate $TbCl_3$ into the buffer, and calculate the free Tb^{3+} concentration by Eq. (8). Excite ProCA at 280 nm, and observe the Tb^{3+}-LRET signal at emission wavelengths between 500 and

650 nm. Calculate the Tb^{3+}-binding affinity for ProCA32 ($K_{d_{\text{Tb, DTPA}}}$) by fitting the Tb^{3+}-LRET signal change over various concentrations of free Tb^{3+} using Eq. (9):

$$\left[\text{Tb}^{3+}\right]_{\text{free}} = K_{d_{\text{Tb, DTPA}}} \times \frac{[\text{Tb} - \text{DTPA}]}{[\text{DTPA}]} \quad (8)$$

$$f = \frac{\left[\text{Tb}^{3+}\right]^n_{\text{free}}}{K^n_{d_{\text{Tb, ProCA}}} + \left[\text{Tb}^{3+}\right]^n_{\text{free}}} \quad (9)$$

where $[Tb^{3+}]_{\text{free}}$ denotes the free Tb^{3+} concentration calculated from the buffer system, $K_{d_{\text{Tb, DTPA}}}$ is the dissociation constant between Tb^{3+} and DTPA, [Tb-DTPA] represents the concentration of Tb-DTPA complex, $[\text{DTPA}]_{\text{free}}$ is the free DTPA concentration in the buffer, f is the fractional change, and $K_{d\text{Tb, ProCA}}$ is the dissociation constant between Tb^{3+} and ProCA32.

3.6 Relaxivity Studies of ProCA32

Measure the relaxation times (T1 and T2) using a Bruker relaxometer at 1.47 T and MRI scanner at 4.7 and 7 T. Prepare the contrast agents at different concentrations in 50 mM HEPES and 100 mM NaCl, pH 7.4. Calculate the relaxivities by Eq. (10):

$$r_i = \frac{\frac{1}{T_{\text{isample}}} - \frac{1}{T_{\text{ibutfer}}}}{[\text{Gd}]_T} \quad i = 1, 2, \quad (10)$$

where r_{i} denotes the per Gd^{3+} relaxivity, T_{isample} is the relaxation time of water after adding ProCA, T_{ibuffer} is the relaxation time of water without adding contrast agents, and $[\text{Gd}]_T$ is the total Gd^{3+} concentration in the tested solution (Fig. 3).

3.7 Determination of Water Coordination Number of ProCA

Determine the number of coordination water molecules in the inner sphere of Gd^{3+}-ProCA by the difference in Tb^{3+} luminescence decay between H_2O and D_2O [35]. Measure the Tb^{3+} lifetime using a fluorescence spectrophotometer.

a. Prepare Tb^{3+}-ProCA complexes in H_2O and D_2O, separately.

b. After excitation at 265 mm, record Tb^{3+} emission decay over time at 545 nm.

c. Fit luminescence decay using monoexponential decay.

d. Establish a standard curve of water number (denoted q) over ΔK_{obs} (the difference of the decay constant between H_2O and D_2O) using well-characterized chelators, such as Tb^{3+}-DTPA ($n = 1$), Tb^{3+}-EDTA ($n = 3$ when [EGTA]:[Tb^{3+}] 1:1), Tb^{3+}-NTA, and Tb^{3+} in aqueous solution ($n = 9$).

e. Calculate the water number of Tb^{3+}-ProCAs by fitting ΔK_{obs} into the standard curve. Obtain the water numbers of Gd-DTPA and Eovist from published studies [36].

3.8 Transmetallation Assay

Consider the transmetallation of Gd^{3+} chelators by physiological ions such as Fe^{3+}, Cu^{2+}, and Zn^{2+} in the development of the contrast agents. Under physiological conditions, Zn^{2+} and PO_4^{3-} are the major molecules to compete with contrast agents for Gd^{3+}. Measure the relaxation rate changes of ProCA32 loaded with different Gd^{3+} ratios in phosphate buffer supplemented with $ZnCl_2$ for different lengths of time. Due to the high relaxivity, reduce both the Gd^{3+} concentration and chelator concentrations to 25–50 times in this study. To better compare the transmetallation properties of ProCA32 with clinical MRI contrast agents, reduce the concentrations of Zn^{2+} and PO_4^{3-} by 25 times.

3.9 Molecular Imaging of PSMA Using Targeted ProCA32

For molecular imaging of PSMA in prostate cancer, a contrast agent should have targeting moieties with affinity at least in the μM range. Moreover, it must have high relaxivity in order to produce significant contrast differences in the tumor site before and after injection of contrast agents. Another important criterion is strong Gd^{3+} affinity and high Gd^{3+} selectivity over physiological metal ions such as Zn^{2+} and Ca^{2+} to prevent free Gd^{3+} from being released, which could result in nephrogenic systemic fibrosis. Additionally, because PSMA is mainly expressed on prostate tumor cells that are far away from the blood vessels, the contrast agent must have strong tumor penetration. Develop the PSMA-targeted ProCA32 by engineering a PSMA-targeting peptide at the C-terminal of ProCA32 (Fig. 1b). Insert a flexible linker between ProCA32 and the targeting peptide to prevent the protein from interfering with the targeting capability of the peptide. Addition of the targeting moiety at the C-terminal of ProCA32 has little effect on the expression and folding of the protein variants. PEGylate the protein to improve its in vivo properties [23]. The incorporation of a PSMA-targeting peptide to ProCA32 with a flexible linker equips ProCA32 with PSMA-targeting capacity while maintaining high metal affinity and selectivity, as well as high relaxivities.

3.10 Parameters of Molecular Imaging with MRI

Collect MR images of the mice on both 4.7 and 7.0 T Varian MR animal scanners. Acquire different MR pulse sequences such as T1-weighted, T2-weighted, and T2 map images. Acquire T1-weighted images using a 2D spin-echo pulse sequence with the following parameters: TR/TE, 400/11 ms; FOV, 4 cm × 4 cm with a matrix size of 512 × 512; slice thickness, 1 mm; and 23 slices. Acquire T2-weighted images using a 2D RARE pulse sequence with the following parameters: TR/TE, 4.4 s/56 ms; FOV, 4 cm × 4 cm with a matrix size of 256 × 256; and slice thickness of 1 mm. Collect The T2 map before the

contrast agent injection and at different time points after IV injection of 5 mM ProCA32 or ProCA32.PSMA using the MSME sequence with the following parameters: TR = 3 s, different length of TE, matrix = 128 × 128, FOV = 4 cm × 3 cm, and slice thickness = 1 mm. Generate the final T2-map images by using an ImageJ plugin MRI T2 calculator (*see* Fig. 4).

4 Notes

1. To ensure that the protein loaded to FPLC is completely apo- or Ca^{2+}-free, incubate the supernatant with 20 mM EGTA for a few hours at 4 °C, and then inject into an FPLC for column binding [22, 23].
2. When different fractions of FPLC are eluting the protein, you should take 20 μL of samples, and mix it with 120 μL of 1 × Bio-Rad Protein Assay solution. If the solution turns blue, the eluent should include the purified protein.
3. To monitor the protein expression and purification process, you are advised to collect samples at each step and analyze them with SDS-PAGE. For example, we always keep 11 samples for SDS-PAGE analysis: cells before induction, cells after induction (1.5 and 3 h), cell pellets after sonication, supernatant before binding and after 85 °C incubation, supernatant after streptomycin/dialysis, fractions after column binding, flow through, and eluent [22, 23].
4. Snap-freeze the cell pellets with liquid nitrogen and store at −80 °C for long-term use. It is strongly suggested to proceed to purification steps in the same day to minimize degradation and/or unfolding of engineered proteins.
5. For α-parvalbumin purification, the pH of 8.0 is important, and it is optimized since it helps the binding of the protein to the HiTrap Q column [22].
6. The 15 min interval between each titration point is essential for reaching full equilibrium between metals and protein in all metal-binding assays. It is important to observe the gradual increase or decrease of luminescence signal until it reaches saturation [22, 23].

Acknowledgments

We appreciate the critical review by Dr. Michael Kirberger and previous works by Drs. Fan Pu, Jingjuan Qiao, and Jie Jiang. This work is supported in part by grants R42 CA183376, R41CA177034, R41AA112713, EB007268, 1R01GM081749 from National Health Institute to Jenny J. Yang. This work was also supported by the Molecular Basis of Disease (MBD) Fellowship to M. Salarian and Center for Diagnostics and Therapeutics (CDT) Fellowship to O. Y. Ibhagui.

References

1. Tyszka JM, Fraser SE, Jacobs RE (2005) Magnetic resonance microscopy: recent advances and applications. Curr Opin Biotechnol 16(1):93–99. 10.1016/j.copbio.2004.11.004 [PubMed: 15722021]
2. Lippard SJ (2006) The inorganic side of chemical biology. Nat Chem Biol 2(10):504–507. 10.1038/nchembio1006-504 [PubMed: 16983380]
3. Lauffer RB, Vincent AC, Padmanabhan S, Villringer A, Saini S, Elmaleh DR, Brady TJ (1987) Hepatobiliary MR contrast agents: 5-substituted iron-EHPG derivatives. Magn Reson Med 4(6):582–590 [PubMed: 3613958]

4. Aime S, Barge A, Cabella C, Crich SG, Gianolio E (2004) Targeting cells with MR imaging probes based on paramagnetic Gd(III) chelates. Curr Pharm Biotechnol 5(6):509–518 [PubMed: 15579040]
5. Burai L, Scopelliti R, Toth E (2002) EuII-cryptate with optimal water exchange and electronic relaxation: a synthon for potential pO2 responsive macromolecular MRI contrast agents. Chem Commun (Camb) 20:2366–2367
6. Geraldes CF, Sherry AD, Cacheris WP, Kuan KT, Brown RD 3rd, Koenig SH, Spiller M (1988) Number of inner-sphere water molecules in Gd^{3+} and Eu^{3+} complexes of DTPA-amide and -ester conjugates. Magn Reson Med 8(2):191–199 [PubMed: 3210956]
7. Caravan P (2006) Strategies for increasing the sensitivity of gadolinium based MRI contrast agents. Chem Soc Rev 35(6):512–523. 10.1039/b510982p [PubMed: 16729145]
8. Weinmann HJ, Press WR, Gries H (1990) Tolerance of extracellular contrast agents for magnetic resonance imaging. Investig Radiol 25 (Suppl 1):S49–S50 [PubMed: 2283256]
9. Opsahl LR, Uzgiris EE, Vera DR (1995) Tumor imaging with a macromolecular paramagnetic contrast agent: gadopentetate dimeglumine-polylysine. Acad Radiol 2(9):762–767 [PubMed: 9419637]
10. Langereis S, de Lussanet QG, van Genderen MH, Meijer EW, Beets-Tan RG, Griffioen AW, van Engelshoven JM, Backes WH (2006) Evaluation of Gd(III)DTPA-terminated poly (propylene imine) dendrimers as contrast agents for MR imaging. NMR Biomed 19(1):133–141. 10.1002/nbm.1015 [PubMed: 16450331]
11. Bryant LH Jr, Brechbiel MW, Wu C, Bulte JW, Herynek V, Frank JA (1999) Synthesis and relaxometry of high-generation (G = 5, 7, 9, and 10) PAMAM dendrimer-DOTA-gadolinium chelates. J Magn Reson Imaging 9(2):348–352 [PubMed: 10077036]
12. Sirlin CB, Vera DR, Corbeil JA, Caballero MB, Buxton RB, Mattrey RF (2004) Gadolinium-DTPA-dextran: a macromolecular MR blood pool contrast agent. Acad Radiol 11(12):1361–1369. 10.1016/j.acra.2004.11.016 [PubMed: 15596374]
13. Lanza GM, Winter PM, Caruthers SD, Morawski AM, Schmieder AH, Crowder KC, Wickline SA (2004) Magnetic resonance molecular imaging with nanoparticles. J Nucl Cardiol 11(6):733–743 [PubMed: 15592197]
14. Lanza GM, Winter P, Caruthers S, Schmeider A, Crowder K, Morawski A, Zhang H, Scott MJ, Wickline SA (2004) Novel paramagnetic contrast agents for molecular imaging and targeted drug delivery. Curr Pharm Biotechnol 5(6):495–507 [PubMed: 15579039]
15. Anderson EA, Isaacman S, Peabody DS, Wang EY, Canary JW, Kirshenbaum K (2006) Viral nanoparticles donning a paramagnetic coat: conjugation of MRI contrast agents to the MS2 capsid. Nano Lett 6(6):1160–1164. 10.1021/nl060378g [PubMed: 16771573]
16. Strijkers GJ, Mulder WJ, van Heeswijk RB, Frederik PM, Bomans P, Magusin PC, Nicolay K (2005) Relaxivity of liposomal paramagnetic MRI contrast agents. MAGMA 18(4):186–192. 10.1007/s10334-005-0111-y [PubMed: 16155762]
17. Stosiek C, Garaschuk O, Holthoff K, Konnerth A (2003) In vivo two-photon calcium imaging of neuronal networks. Proc Natl Acad Sci U S A 100(12):7319–7324. 10.1073/pnas.1232232100 [PubMed: 12777621]
18. Wallingford JB, Ewald AJ, Harland RM, Fraser SE (2001) Calcium signaling during convergent extension in Xenopus. Curr Biol 11(9):652–661 [PubMed: 11369228]
19. Caravan P, Greenwood JM, Welch JT, Franklin SJ (2003) Gadolinium-binding helix-turn-helix peptides: DNA-dependent MRI contrast agents. Chem Commun (Camb) 20:2574–2575
20. Kim Y, Welch JT, Lindstrom KM, Franklin SJ (2001) Chimeric HTH motifs based on EF-hands. J Biol Inorg Chem 6(2):173–181 [PubMed: 11293411]
21. Atanasijevic T, Shusteff M, Fam P, Jasanoff A (2006) Calcium-sensitive MRI contrast agents based on superparamagnetic iron oxide nanoparticles and calmodulin. Proc Natl Acad Sci U S A 103(40):14707–14712. 10.1073/pnas.0606749103 [PubMed: 17003117]
22. Xue S, Yang H, Qiao J, Pu F, Jiang J, Hubbard K, Hekmatyar K, Langley J, Salarian M, Long RC, Bryant RG, Hu XP, Grossniklaus HE, Liu ZR, Yang JJ (2015) Protein MRI contrast agent with unprecedented metal selectivity and sensitivity for liver cancer imaging. Proc Natl Acad Sci U S A 112(21):6607–6612. 10.1073/pnas.1423021112 [PubMed: 25971726]

23. Pu F, Salarian M, Xue S, Qiao J, Feng J, Tan S, Patel A, Li X, Mamouni K, Hekmatyar K, Zou J, Wu D, Yang JJ (2016) Prostate-specific membrane antigen targeted protein contrast agents for molecular imaging of prostate cancer by MRI. Nanoscale 8(25):12668–12682. 10.1039/c5nr09071g [PubMed: 26961235]
24. Pu F, Qiao J, Xue S, Yang H, Patel A, Wei L, Hekmatyar K, Salarian M, Grossniklaus HE, Liu ZR, Yang JJ (2015) GRPR-targeted protein contrast agents for molecular imaging of receptor expression in cancers by MRI. Sci Rep 5:16214 10.1038/srep16214 [PubMed: 26577829]
25. Xue S, Qiao J, Jiang J, Hubbard K, White N, Wei L, Li S, Liu ZR, Yang JJ (2014) Design of ProCAs (protein-based Gd(3+) MRI contrast agents) with high dose efficiency and capability for molecular imaging of cancer biomarkers. Med Res Rev 34(5):1070–1099. 10.1002/med.21313 [PubMed: 24615853]
26. Qiao J, Xue S, Pu F, White N, Jiang J, Liu ZR, Yang JJ (2014) Molecular imaging of EGFR/HER2 cancer biomarkers by protein MRI contrast agents. J Biol Inorg Chem 19(2):259–270. 10.1007/s00775-013-1076-3 [PubMed: 24366655]
27. Li S, Jiang J, Zou J, Qiao J, Xue S, Wei L, Long R, Wang L, Castiblanco A, White N, Ngo J, Mao H, Liu ZR, Yang JJ (2012) PEGylation of protein-based MRI contrast agents improves relaxivities and biocompatibilities. J Inorg Biochem 107(1):111–118. 10.1016/j.jinorgbio.2011.11.004 [PubMed: 22178673]
28. Pu F, Xue S, Qiao J, Patel A, Yang JJ (2016) Towards the Molecular Imaging of Prostate Cancer Biomarkers Using Protein-based MRI Contrast Agents. Curr Protein Pept Sci 17(6):519–533 [PubMed: 26721404]
29. Wang X, Kirberger M, Qiu F, Chen G, Yang JJ (2009) Towards predicting Ca^{2+}–binding sites with different coordination numbers in proteins with atomic resolution. Proteins 75(4):787–798. 10.1002/prot.22285 [PubMed: 19003991]
30. Kirberger M, Wang X, Deng H, Yang W, Chen G, Yang JJ (2008) Statistical analysis of structural characteristics of protein Ca^{2+}–binding sites. J Biol Inorg Chem 13 (7):1169–1181. 10.1007/s00775-008-0402-7 [PubMed: 18594878]
31. Wang X, Zhao K, Kirberger M, Wong H, Chen G, Yang JJ (2010) Analysis and prediction of calcium-binding pockets from apo-protein structures exhibiting calcium-induced localized conformational changes. Protein Sci 19(6):1180–1190. 10.1002/pro.394 [PubMed: 20512971]
32. Zhou Y, Yang W, Kirberger M, Lee HW, Ayalasomayajula G, Yang JJ (2006) Prediction of EF-hand calcium-binding proteins and analysis of bacterial EF-hand proteins. Proteins 65(3):643–655. 10.1002/prot.21139 [PubMed: 16981205]
33. Dees A, Zahl A, Puchta R, Hommes NJ, Heinemann FW, Ivanovic-Burmazovic I (2007) Water exchange on seven-coordinate Mn(II) complexes with macrocyclic pentadentate ligands: insight in the mechanism of Mn(II) SOD mimetics. Inorg Chem 46(7):2459–2470. 10.1021/ic061852o [PubMed: 17326621]
34. Grynkiewicz G, Poenie M, Tsien RY (1985) A new generation of Ca^{2+} indicators with greatly improved fluorescence properties. J Biol Chem 260(6):3440–3450 [PubMed: 3838314]
35. Sudnick DR, Horrocks WD Jr (1979) Lanthanide ion probes of structure in biology. Environmentally sensitive fine structure in laser-induced terbium(III) luminescence. Biochim Biophys Acta 578(1):135–144 [PubMed: 454662]
36. Caravan P, Ellison JJ, McMurry TJ, Lauffer RB (1999) Gadolinium(III) chelates as MRI contrast agents: structure, dynamics, and applications. Chem Rev 99(9):2293–2352 [PubMed: 11749483]

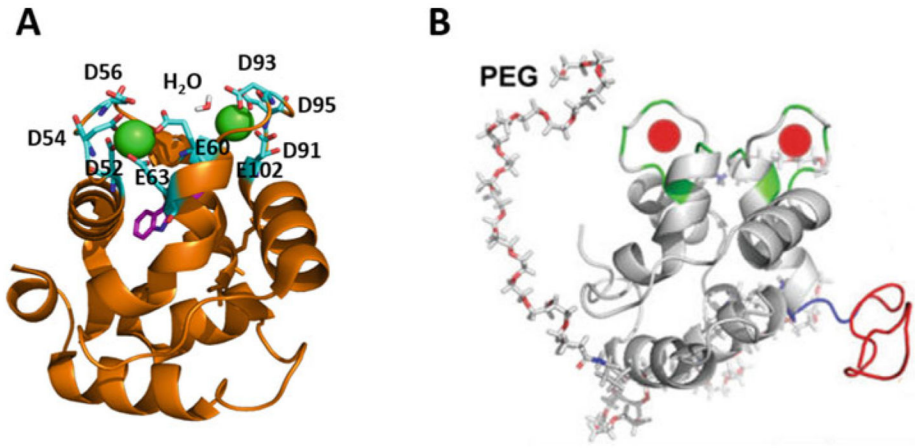

Fig. 1.

(**a**) Model structure of ProCA32 based on α-parvalbumin. (**b**) Model structure of PEGylated PSMA-targeted ProCA32 for the molecular imaging of PSMA in prostate cancer

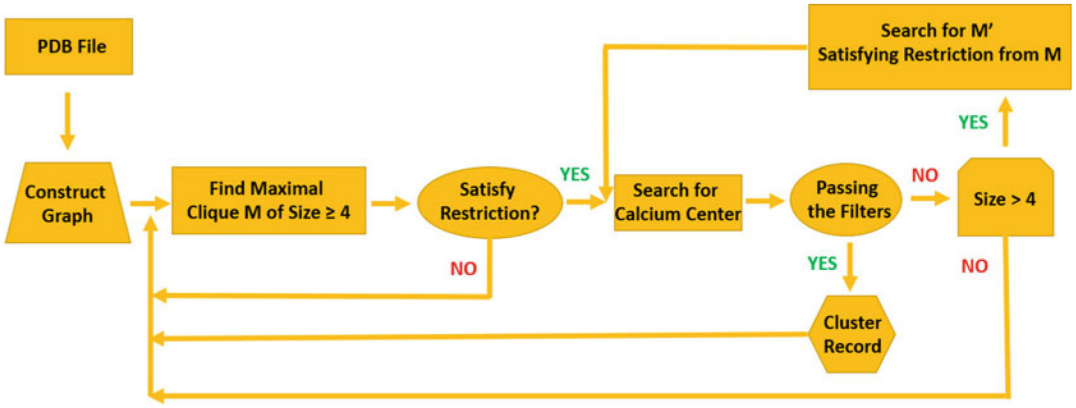

Fig. 2.

Flow chart of MUG algorithm for prediction of Gd^{3+}- and Ca^{2+}-binding sites in CaBPs. Restriction: a cluster must have at least four oxygen atoms of specified types where at least *n* (*n* = 2, 3, 4) oxygen atoms are from amino acids. Both the type and n are the input parameters

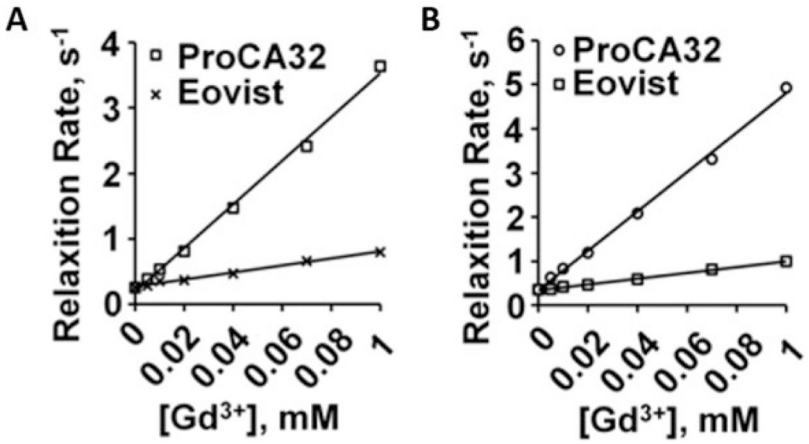

Fig. 3.

(**a**) Changes in R_1 relaxation rate over different concentrations of Gd^{3+} in ProCA32 and clinical contrast agent, Eovist at 1.5 T and 37 °C. (**b**) Changes in R_2 relaxation rate over different concentrations of Gd^{3+} in ProCA32 and Eovist at1.5 T and 37 °C

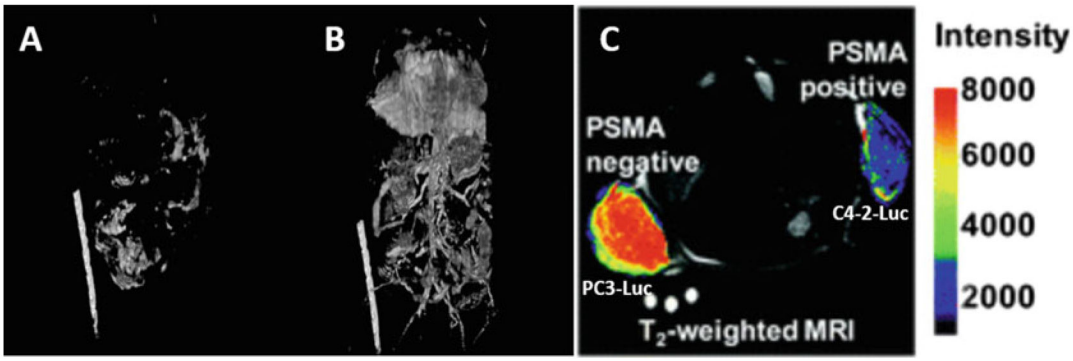

Fig. 4.

Three-dimensional MRI of mouse (**a**) before and (**b**) after injection of ProCA32. The bright line next to the mouse is a tube filled with the contrast agent as a reference. (**c**) MR imaging of PSMA in xenografted mice tumors by PSMA-targeted ProCA32 (ProCA32.PSMA). T2-weighted MRI of the mice implanted with both PC3-Luc and C4–2-Luc tumors after injection of ProCA32.PSMA were collected. The PSMA-positive tumor, C4–2-Luc, exhibited decreased MRI signal intensity at 30 min–48 h postinjection of ProCA32.PSMA, while the PSMA-negative tumor, PC3-Luc, did not show any significant MRI signal change